
AN OSRC PRECONDITIONER FOR THE EFIE

Ignacia Fierro-Piccardo
 Department of Mathematics
 University College London
 London, WC1E 6BT, U.K.
 maria.piccardo.19@ucl.ac.uk

Timo Betcke
 Department of Mathematics
 University College London
 London, WC1E 6BT, U.K.
 t.betcke@ucl.ac.uk

ABSTRACT

The Electric Field Integral Equation (EFIE) is a well-established tool to solve scattering problems. But the development of efficient and easy to implement preconditioners remains an active research area. In recent years, operator preconditioning approaches have become popular for the EFIE, where the electric field operator is regularised by multiplication with another convenient operator. A particularly intriguing choice is the exact Magnetic-to-Electric (MtE) operator as regulariser. However, evaluating this operator is as expensive as solving the original EFIE. In a work by El Bouajaji, Antoine and Geuzaine approximate local Magnetic-to-Electric surface operators for the time-harmonic Maxwell equation were proposed that can be efficiently evaluated through the solution of sparse surface problems. This paper demonstrates the preconditioning properties of these approximate MtE operators for the EFIE. The implementation is described and a number of numerical comparisons against other preconditioning techniques for the EFIE are presented to demonstrate the effectiveness of this new technique.

Keywords Preconditioner, Boundary Integral Equations, Boundary Elements Method, OSRC approximation, Electric Field Integral Equation.

1 Introduction

The numerical simulation of time-harmonic waves scattered from perfect electric conductors (PECs) is of fundamental importance across the spectrum of electromagnetic applications.

Denote by \mathbf{e}^{inc} an incident field. We are looking for the solution $\mathbf{e}^{\text{tot}} = \mathbf{e}^{\text{inc}} + \mathbf{e}^{\text{scat}}$ of the exterior scattering problem, satisfying

$$\mathbf{curl} \mathbf{curl} \mathbf{e}^{\text{tot}} - \kappa^2 \mathbf{e}^{\text{tot}} = 0 \quad \text{in } \Omega^+, \quad (1a)$$

$$\mathbf{e}^{\text{tot}} \times \boldsymbol{\nu} = 0 \quad \text{on } \Gamma, \quad (1b)$$

$$\lim_{|\mathbf{x}| \rightarrow \infty} |\mathbf{x}| \left(\mathbf{curl} \mathbf{e}^{\text{scat}} \times \frac{\mathbf{x}}{|\mathbf{x}|} - i\kappa \mathbf{e}^{\text{scat}} \right) = 0. \quad (1c)$$

Here, $\kappa = \omega \sqrt{\epsilon_0 \mu_0}$ denotes the wavenumber of the problem, with ω denoting the frequency and ϵ_0 and μ_0 the electric permeability and magnetic permittivity in vacuum. The PEC object is denoted by $\Omega^- \subset \mathbb{R}^3$ and it is enclosed by a smooth boundary $\Gamma = \partial\Omega^-$, also $\Omega^+ = \mathbb{R}^3 \setminus \overline{\Omega^-}$ denotes the propagation medium. Frequently, the incident field is a plane wave given by $\mathbf{e}^{\text{inc}} = \mathbf{p} e^{i\kappa \mathbf{x} \cdot \mathbf{d}}$, where \mathbf{p} is a non-zero vector representing the polarisation of the wave and \mathbf{d} is a unit vector perpendicular to \mathbf{p} that gives the direction of the plane wave.

The simulation of time-harmonic waves scattered from perfect electric conductors (PECs) is a key application area for boundary element methods as they naturally deal with the infinite domain problem by reducing the computation of the numerical solution of an integral equation on a finite dimensional surface. In the low-frequency regime a direct solution

of the electric field integral equation (EFIE) is well established (see [7]). As the mesh width decreases, however, the formulation suffers from ill-conditioning, hence a regulariser, \mathbf{R} is needed:

$$\mathbf{R}\mathbf{S}_\kappa\gamma_N^+\mathbf{e} = -\mathbf{R}\left(\frac{\mathbf{I}}{2} + \mathbf{C}_\kappa\right)\gamma_t^+\mathbf{e}^{inc} \quad (2)$$

Here, a direct formulation of the EFIE has been presented, with \mathbf{S}_κ as the electric field integral operator and \mathbf{C}_κ as the magnetic field integral operator. In the most simple form \mathbf{R} is just an inverse diagonal or an algebraic preconditioner, but more sophisticated implementations are based on the idea of choosing \mathbf{R} as the discretisation of an operator that regularises the electric field operator \mathbf{S}_κ in continuous spaces [4].

The most common example of \mathbf{R} is the Calderón Multiplicative Preconditioner [1] and difficulty here is the evaluation of operator products. Assume a function ϕ in some Hilbert space, and operators \mathbf{A} and \mathbf{B} in compatible Hilbert spaces. In order to evaluate the product $\psi = \mathbf{A}\mathbf{B}\phi$ through Galerkin discretisations of the operators \mathbf{A} and \mathbf{B} we need to compute a finite dimensional matrix product of the form $\psi_h = \mathbf{A}_h\mathbf{M}_h^{-1}\mathbf{B}_h\phi_h$, where we have used the subscript h to denote finite dimensional quantities after discretisation [5]. The matrix \mathbf{M}_h is a mass matrix, which contains the inner product of the test space of \mathbf{B}_h and the domain space of \mathbf{A}_h . The difficulty is that this mass matrix is numerically singular for the standard choice of RWG spaces in electromagnetic scattering [6], a problem that does not occur for simple P1 spaces used in many acoustic problems. In order to overcome this problem one can use so-called Buffa-Christiansen (BC) spaces as test spaces [1]. However, their use is expensive due to the requirement of barycentric refinements. One aim of this research is to build a preconditioner that avoids the use of BC spaces and that can simply be defined using RWG spaces in the primal grid.

Aiming to avoid the use of BC spaces, the optimal operator \mathbf{R} to use as a regulariser has been considered to be the Magnetic-to-Electric (MtE) operator. It turns out that with this choice the left-hand side of (2) becomes a second kind integral operator, thus in theory, making it much more amenable to iterative solvers. However, a direct evaluation of the MtE operator has a similar complexity to solving the original scattering problem. It is therefore not practical. In the early 2000s Antoine, Darbas, and their co-authors investigated in the acoustic scattering case a class of approximations to the Dirichlet-to-Neumann (DtN) map based on Padé expansions of high-frequency approximations of this operator. It turns out that this OSRC method (On-Surface-Radiation Condition) allows an accurate approximation of the DtN map and its inverse simply by solving sparse surface linear systems of equations on the boundary of the scatterer (see [3, 2, 8], and [11] for earlier work by Kiregsmann, Taflove and Umashankar).

In recent work by Bouajaji, Antoine, and Geuzaine this OSRC concept was extended to the MtE operator in three dimensional electromagnetic scattering, allowing it to be well approximated by the solution of sparse linear systems arising from surface differential operators [9].

In this paper we follow this approach for approximating the MtE operator and investigate the suitability of this approximation as regulariser for the EFIE. We also demonstrate details of the implementation and the resulting preconditioning performance with respect to time and matrix-vector products.

The paper is organised as follows: in section 2 an overview of physical problem and function spaces for Maxwell boundary integral operators is presented. Section 3 shows the MtE preconditioner and its continuous implementation and approximations, while section 4 shows the discrete implementation of MtE as a preconditioner. Section 5 presents a validation of this new preconditioner and some tests on its performance, with conclusion given in section 6.

2 Problem setting, Tangential Sobolev Spaces and Surface Operators

2.1 Function Spaces

To solve the problem in (19), consider the definition of generic Sobolev spaces on Ω^\pm :

$$\mathbf{H}_{loc}^s(\mathbf{d}, \Omega^\pm) := \{\mathbf{u} \in \mathbf{H}_{loc}^s(\Omega^\pm) \mid \mathbf{d} \mathbf{u} \in \mathbf{H}_{loc}^s(\Omega^\pm)\}.$$

Here \mathbf{d} is a pseudodifferential operator, the sub-fix $_{loc}$ stands for the assumption of integrability within all compact subsets in Ω^\pm (which is not necessary when Ω^\pm is bounded. In that case, $\mathbf{H}_{loc}(\mathbf{d}, \Omega^\pm)$ is replaced by $\mathbf{H}(\mathbf{d}, \Omega^\pm)$). However, in order to formulate boundary value problems for Maxwell's equations, it is necessary to define spaces on the boundary, hence the tangential, magnetic and Neuman traces are given respectively by:

$$\begin{aligned}\gamma_t^\pm \mathbf{p} &:= \lim_{\Omega^\pm \ni \mathbf{x}' \rightarrow \mathbf{x} \in \Gamma} \mathbf{p}(\mathbf{x}') \times \boldsymbol{\nu}(\mathbf{x}) \\ \gamma_N^\pm \mathbf{q} &:= \kappa^{-1} \gamma_t^\pm \mathbf{curl} \mathbf{q}(\mathbf{x}') \\ \gamma_\nu^\pm \mathbf{w} &:= \lim_{\Omega^\pm \ni \mathbf{x}' \rightarrow \mathbf{x} \in \Gamma} \mathbf{w}(\mathbf{x}') \cdot \boldsymbol{\nu}(\mathbf{x})\end{aligned}$$

for $\mathbf{p} \in \mathbf{H}_{loc}(\mathbf{curl}, \Omega^\pm)$, $\mathbf{q} \in \mathbf{H}_{loc}(\mathbf{curl}^2, \Omega^\pm)$, and $\mathbf{w} \in \mathbf{H}_{loc}(\mathbf{div}, \Omega^\pm)$.

As stated in [7], Green's formula implies the definition of the tangential trace on Γ :

$$\int_{\Omega} (\mathbf{u} \cdot \mathbf{curl} \mathbf{v} - \mathbf{v} \cdot \mathbf{curl} \mathbf{u}) d\Omega = \int_{\Gamma} \gamma_t \mathbf{u} \cdot \mathbf{v} d\Gamma \quad (3)$$

with $\mathbf{u} \in \mathbf{H}_{loc}(\mathbf{curl}, \Omega^\pm)$, $\mathbf{v} \in \mathbf{H}^1(\Omega)$. Since $\gamma : \mathbf{H}^1(\Omega) \rightarrow \mathbf{H}^{\frac{1}{2}}(\Gamma)$ is surjective, then [7] defines the following space for smooth surfaces:

$$\mathbf{H}^{\frac{1}{2}}(\Gamma) := \gamma_t^-(\mathbf{H}^1(\Omega^-)) = \{\gamma_t^- \mathbf{u} : \mathbf{u} \in \mathbf{H}^1(\Omega^-)\} \quad (4)$$

and from (3) it is natural to define $\mathbf{H}^{-\frac{1}{2}}(\Gamma)$ as the dual space of $\mathbf{H}^{\frac{1}{2}}(\Gamma)$. Hence $\gamma_t : \mathbf{H}_{loc}(\mathbf{curl}, \Omega^\pm) \rightarrow \mathbf{H}^{-\frac{1}{2}}(\Gamma)$, is well-defined and continuous. Also, the scalar surface divergence of $\gamma_t^\pm \mathbf{u}$, for $\mathbf{u} \in \mathbf{H}_{loc}(\mathbf{curl}, \Omega^\pm)$ is defined as $\mathbf{Div}_\Gamma(\gamma_t^\pm \mathbf{u}) = \gamma_\nu^\pm(\mathbf{curl}(\mathbf{u}))$. Therefore, on a smooth domain we have: $\gamma_t : \mathbf{H}_{loc}(\mathbf{curl}, \Omega^\pm) \rightarrow \mathbf{H}^{-\frac{1}{2}}(\mathbf{Div}_\Gamma, \Gamma)$. Since this is not obvious for non-smooth domains [7], in order to build a the Galerkin formulation, it is assumed that the grid over Γ consists of a finite union of smooth faces ($\Gamma = \cup_{j=0}^m \Gamma^j$). Hence, according to [7, definition 1] $\mathbf{H}^{\frac{1}{2}}(\Gamma)$ is replaced by $\mathbf{H}_\times^{\frac{1}{2}}(\Gamma) \subset \mathbf{L}_t^2(\Gamma)$, which preserves the definition in (4): $\mathbf{H}_\times^{\frac{1}{2}}(\Gamma) := \gamma_t^-(\mathbf{H}^1(\Omega^-)) = \{\gamma_t^- \mathbf{u} : \mathbf{u} \in \mathbf{H}^1(\Omega^-)\}$ (here $\mathbf{L}_t^2(\Gamma) := \{\mathbf{u} \in \mathbf{L}^2(\Gamma) : \mathbf{u} \cdot \boldsymbol{\nu} = 0\}$ defines the tangential space of square integrable functions).

Notice that for $\mathbf{u} \in \mathbf{H}_{loc}(\mathbf{curl}, \Omega^\pm)$, considering the dual pairing in (3), it is possible to define $\mathbf{H}_\times^{-\frac{1}{2}}(\mathbf{Div}_\Gamma, \Gamma)$ as its self dual with respect to $\mathbf{L}_t^2(\Gamma)$ as a pivot space. For the same reason $\mathbf{H}_\times^{-\frac{1}{2}}(\mathbf{curl}_\Gamma, \Gamma)$ becomes the dual of $\mathbf{H}_\times^{-\frac{1}{2}}(\mathbf{Div}_\Gamma, \Gamma)$ respect to the standard $\mathbf{L}_t^2(\Gamma)$ dual product. To complete the description of the properties of the tangential and magnetic traces, it is necessary to remark that $\gamma_t^\pm : \mathbf{H}_{loc}(\mathbf{curl}, \Omega^\pm) \rightarrow \mathbf{H}_\times^{-\frac{1}{2}}(\mathbf{Div}_\Gamma, \Gamma)$ and $\gamma_N^\pm : \mathbf{H}_{loc}(\mathbf{curl}^2, \Omega^\pm) \rightarrow \mathbf{H}_\times^{-\frac{1}{2}}(\mathbf{Div}_\Gamma, \Gamma)$ are continuous and subjective ([7, Lemma 3]) on finite domains.

2.2 Operators

To solve (1), the Stratton-Chu representation formulas [12] must be considered for any $\mathbf{x} \in \Omega^+$:

$$\mathbf{e}(\mathbf{x}) := -\mathcal{T}([\gamma_t]_\Gamma \mathbf{e})(\mathbf{x}) - \mathcal{K}([\gamma_N]_\Gamma \mathbf{e})(\mathbf{x}) \quad (5)$$

where $\mathcal{T}, \mathcal{K} : \mathbf{H}_\times^{-\frac{1}{2}}(\mathbf{Div}_\Gamma, \Gamma) \rightarrow \mathbf{H}_{loc}(\mathbf{curl}^2, \Omega^+ \cup \Omega^-)$ are defined as:

$$\begin{aligned}\mathcal{T}(\mathbf{p})(\mathbf{x}) &:= i\kappa \int_{\Gamma} \mathbf{p}(\mathbf{y}) \mathbf{G}(\mathbf{x}, \mathbf{y}) - \frac{1}{i\kappa} \nabla_{\mathbf{x}} \int_{\Gamma} \mathbf{G}(\mathbf{x}, \mathbf{y}) \mathbf{Div}_\Gamma \mathbf{p}(\mathbf{y}) d\Gamma(\mathbf{y}), \\ \mathcal{K}(\mathbf{p})(\mathbf{x}) &:= \mathbf{curl}_{\mathbf{x}} \int_{\Gamma} \mathbf{G}(\mathbf{x}, \mathbf{y}) \mathbf{p}(\mathbf{y}) d\Gamma(\mathbf{y})\end{aligned}$$

With $\mathbf{G}(\mathbf{x}, \mathbf{y}) := \frac{e^{i\kappa \|\mathbf{x} - \mathbf{y}\|}}{4\|\mathbf{x} - \mathbf{y}\|}$, $\mathbf{x} \neq \mathbf{y}$.

By applying magnetic and tangential traces to the Electric and Magnetic field potential operators the electric and magnetic BIOs $\mathbf{S}_\kappa, \mathbf{C}_\kappa : \mathbf{H}_\times^{-\frac{1}{2}}(\mathbf{Div}_\Gamma, \Gamma) \rightarrow \mathbf{H}^{-\frac{1}{2}}(\mathbf{Div}_\Gamma, \Gamma)$ can be obtained:

$$\begin{aligned}
 \{\gamma_t\}_\Gamma \mathcal{T} &= \mathbf{S}_\kappa & [\gamma_t]_\Gamma \mathcal{T} &= 0 \\
 \{\gamma_t\}_\Gamma \mathcal{K} &= \mathbf{C}_\kappa & [\gamma_t]_\Gamma \mathcal{K} &= -\mathbf{I} \\
 \{\gamma_N\}_\Gamma \mathcal{T} &= \mathbf{C}_\kappa & [\gamma_N]_\Gamma \mathcal{T} &= -\mathbf{I} \\
 \{\gamma_N\}_\Gamma \mathcal{K} &= -\mathbf{S}_\kappa & [\gamma_N]_\Gamma \mathcal{K} &= 0 \\
 \gamma_t^- \mathcal{T} &= \mathbf{S}_\kappa & \gamma_t^+ \mathcal{T} &= \mathbf{S}_\kappa \\
 \gamma_t^- \mathcal{K} &= \frac{\mathbf{I}}{2} + \mathbf{C}_\kappa & \gamma_t^+ \mathcal{K} &= -\frac{\mathbf{I}}{2} + \mathbf{C}_\kappa \\
 \gamma_N^- \mathcal{T} &= \frac{\mathbf{I}}{2} + \mathbf{C}_\kappa & \gamma_N^+ \mathcal{T} &= -\frac{\mathbf{I}}{2} + \mathbf{C}_\kappa \\
 \gamma_N^- \mathcal{K} &= -\mathbf{S}_\kappa & \gamma_N^+ \mathcal{K} &= -\mathbf{S}_\kappa
 \end{aligned}$$

Then, applying electric and magnetic traces to the representation formula (5), the following can be derived:

$$\mathcal{C}^\pm = \begin{bmatrix} \frac{\mathbf{I}}{2} \mp \mathbf{C}_\kappa & \mp \mathbf{S}_\kappa \\ \pm \mathbf{S}_\kappa & \frac{\mathbf{I}}{2} \mp \mathbf{C}_\kappa \end{bmatrix} \begin{bmatrix} \gamma_t^\pm \mathbf{u} \\ \gamma_N^\pm \mathbf{u} \end{bmatrix} = \begin{bmatrix} \gamma_t^\pm \mathbf{u} \\ \gamma_N^\pm \mathbf{u} \end{bmatrix} \quad (6)$$

This is the so called Calderon projector, which allows to find the electric and magnetic fields in the space, from a boundary condition, $\gamma_t^\pm \mathbf{u}$ or $\gamma_N^\pm \mathbf{u}$. This Projector has some important properties, for instance: $(\mathcal{C}^\pm)^2 = \mathcal{C}^\pm$ from which the following can be deduced:

$$\mathbf{S}_\kappa^2 = \mathbf{C}_\kappa^2 - \frac{\mathbf{I}}{4} \quad (7)$$

This is the basis for Calderón Preconditioning. It basically states that \mathbf{S}_κ^2 equals the identity plus a compact operator (a second kind Fredholm operator [10]). Since the spectrum of compact operators clusters at 0, the addition of the identity and this compact operator results in a third operator that in terms of spectral properties will remain stable when discretised. The difficulties of building the discrete version operator arise when trying to build gram matrices \mathbf{G} to implement the discrete product $\mathbf{S}_{\kappa,h} \mathbf{G}^{-1} \mathbf{S}_{\kappa,h}$. These matrices are unstable due to the nature of the discrete spaces used in their construction, so to overcome this problem a CMP has been proposed in [1] and has become standard when building a CP. However, as it was pointed out in the introduction, this technique requires the use of BC basis functions, which translates into an increase of computational complexity of the algorithm, hence the intention to build alternative preconditioners.

3 Construction of an OSRC Preconditioner

In this section we show that the exact Magnetic to Electric (MtE) operator and its inverse (EtM) constitute perfect preconditioners and with this, establish the basic idea of the behavior of an approximate OSRC operator as a preconditioner.

3.1 OSRC operator as a preconditioner for the EFIE

Starting with the exact EtM (Electric to Magnetic) operator, this can be derived from the first row of the Calderon Projector (6):

$$-\mathbf{S}_\kappa^{-1} \left(\frac{\mathbf{I}}{2} + \mathbf{C}_\kappa \right) \gamma_t^+ \mathbf{u} = \gamma_N^+ \mathbf{u}$$

hence the EtM and its inverse (MtE, Magnetic to Electric) operator are given by:

$$\mathbf{V}_{(1)} = -\mathbf{S}_\kappa^{-1} \left(\frac{\mathbf{I}}{2} + \mathbf{C}_\kappa \right) \quad (8)$$

$$\mathbf{V}_{(1)}^{-1} = - \left(\frac{\mathbf{I}}{2} + \mathbf{C}_\kappa \right)^{-1} \mathbf{S}_\kappa \quad (9)$$

And from the second row :

$$\left(\frac{\mathbf{I}}{2} + \mathbf{C}_\kappa \right)^{-1} \mathbf{S}_\kappa \gamma_t^+ \mathbf{u} = \gamma_N^+ \mathbf{u}$$

a second version of the EtM exact operator and its inverse (MtE) is obtained:

$$\mathbf{V}_{(2)} = \left(\frac{\mathbf{I}}{2} + \mathbf{C}_\kappa \right)^{-1} \mathbf{S}_\kappa \quad (10)$$

$$\mathbf{V}_{(2)}^{-1} = \mathbf{S}_\kappa^{-1} \left(\frac{\mathbf{I}}{2} + \mathbf{C}_\kappa \right) \quad (11)$$

An important fact to bear in mind when deriving these expressions is that it is assumed that either \mathbf{S}_κ or $\frac{\mathbf{I}}{2} + \mathbf{C}_\kappa$ are invertible operators when required.

It is necessary to remark that the discrete versions of the pairs (8), (11) and (9), (10) are not necessarily the same, since they might be defined on different discrete spaces. For example, if the electric data is represented in an RWG space and the magnetic data in a BC space [14] possible domain and range pairing of (8), (11) are (RWG, BC) and (BC, RWG) respectively and for (9), (10) are (BC, RWG) and (RWG, BC), also respectively.¹ To discriminate these versions of the \mathbf{V}^{-1} operator we have used the subscripts ₍₁₎ and ₍₂₎ and we state the following:

Theorem 1. *Assuming that Γ is smooth and that κ^2 is not an interior eigenvalue, the following holds for the regularised EFIE:*

$$\mathbf{S}_\kappa \mathbf{V}_{(2)}^{-1} \equiv \left(\frac{\mathbf{I}}{2} + \mathbf{C}_\kappa \right)$$

and

$$\mathbf{V}_{(1)}^{-1} \mathbf{S}_\kappa \equiv \left(\frac{\mathbf{I}}{2} - \mathbf{C}_\kappa \right)$$

where $\mathbf{V}^{-1} : \mathbf{H}_\times^{-\frac{1}{2}}(\mathbf{Div}_\Gamma, \Gamma) \rightarrow \mathbf{H}_\times^{-\frac{1}{2}}(\mathbf{Div}_\Gamma, \Gamma)$ is the inverse MtE operator. In other words, \mathbf{V}^{-1} is a preconditioner.

Proof. The application of the inverse MtE operator to the EFIE operator by the right leads directly to an operator with better spectral properties:

$$\mathbf{S}_\kappa \mathbf{V}_{(2)}^{-1} = \mathbf{S}_\kappa \mathbf{S}_\kappa^{-1} \left(\frac{\mathbf{I}}{2} + \mathbf{C}_\kappa \right) = \left(\frac{\mathbf{I}}{2} + \mathbf{C}_\kappa \right)$$

On the other hand, the inverse MtE applied from the left gives:

$$\mathbf{V}_{(1)}^{-1} \mathbf{S}_\kappa = - \left(\frac{\mathbf{I}}{2} + \mathbf{C}_\kappa \right)^{-1} \mathbf{S}_\kappa \mathbf{S}_\kappa$$

From (7) we have that $\mathbf{S}_\kappa^2 = - \left(\frac{\mathbf{I}}{2} + \mathbf{C}_\kappa \right) \left(\frac{\mathbf{I}}{2} - \mathbf{C}_\kappa \right)$. Then:

¹Here RWG stands for Rao Wilton Glisson basis functions

$$\underbrace{-\left(\frac{\mathbf{I}}{2} + \mathbf{C}_\kappa\right)^{-1} \mathbf{S}_\kappa \mathbf{S}_\kappa}_{\mathbf{V}_{(1)}^{-1}} = \left(\frac{\mathbf{I}}{2} - \mathbf{C}_\kappa\right).$$

Hence, $\left(\frac{\mathbf{I}}{2} - \mathbf{C}_\kappa\right) = \mathbf{V}_{(1)}^{-1} \mathbf{S}_\kappa$.

As a conclusion, $\mathbf{V}_{(1)}^{-1} \mathbf{S}_\kappa$ and $\mathbf{S}_\kappa \mathbf{V}_{(2)}^{-1}$ are equivalent to second kind Fredholm operators.

□

From now on, we drop the subscripts and we refer to $\mathbf{V}_{(1)}^{-1}$ just as \mathbf{V}^{-1} .

From the last theorem, the MtE operator would be an ideal alternative as a preconditioner, $\mathbf{R} = -\mathbf{V}^{-1}$:

$$\mathbf{V}^{-1} \mathbf{S}_\kappa \gamma_N^+ \mathbf{u} = -\mathbf{V}^{-1} \left(\frac{\mathbf{I}}{2} + \mathbf{C}_\kappa\right) \gamma_t^+ \mathbf{u} \quad (12)$$

However, the construction of \mathbf{V}^{-1} is as expensive as solving the EFIE, so finding a good approximation is essential.

3.2 Approximation of the MtE operator ($\mathbf{V}_\varepsilon^{-1}$)

[9] shows that an approximation for the EtM on smooth surfaces is given by

$$\gamma_N^+ \mathbf{u} = \mathbf{\Lambda}^{ex} (\nu \times \gamma_t^+ \mathbf{u}) \quad \text{on } \Gamma,$$

where $\mathbf{\Lambda}^{ex} := \mathbf{\Lambda}_{1,\varepsilon}^{-1} \mathbf{\Lambda}_{2,\varepsilon}$ is given by

$$\mathbf{\Lambda}_{2,\varepsilon} := \mathbf{I} - \mathbf{curl}_\Gamma \frac{1}{\kappa_{\varepsilon opt}^2} \mathbf{curl}_\Gamma : \mathbf{H}_\times^{-\frac{1}{2}}(\mathbf{curl}_\Gamma, \Gamma) \rightarrow \mathbf{H}_\times^{-\frac{1}{2}}(\mathbf{Div}_\Gamma, \Gamma),$$

and

$$\mathbf{\Lambda}_{1,\varepsilon} := (\mathbf{I} + \mathcal{J})^{1/2} : \mathbf{H}_\times^{-\frac{1}{2}}(\mathbf{curl}_\Gamma, \Gamma) \rightarrow \mathbf{H}_\times^{-\frac{1}{2}}(\mathbf{Div}_\Gamma, \Gamma)$$

with

$$\mathcal{J} := \mathbf{Grad}_\Gamma \frac{1}{\kappa_\varepsilon^2} \mathbf{Div}_\Gamma - \mathbf{curl}_\Gamma \frac{1}{\kappa_\varepsilon^2} \mathbf{curl}_\Gamma \quad (13)$$

Hence $\mathbf{\Lambda}^{ex} : \mathbf{H}_\times^{-\frac{1}{2}}(\mathbf{curl}_\Gamma, \Gamma) \rightarrow \mathbf{H}_\times^{-\frac{1}{2}}(\mathbf{curl}_\Gamma, \Gamma)$. However, in order to implement the MtE operator as a preconditioner for the CFIE as in (12), it is required to modify the mapping properties of the MtE operator in such a way such that it maps from $\mathbf{H}_\times^{-\frac{1}{2}}(\mathbf{Div}_\Gamma, \Gamma)$ to $\mathbf{H}_\times^{-\frac{1}{2}}(\mathbf{Div}_\Gamma, \Gamma)$. Therefore, it is necessary to define two auxiliary maps,

$$\begin{aligned} \mathbf{\Theta}_1 &: \mathbf{H}_\times^{-\frac{1}{2}}(\mathbf{Div}_\Gamma, \Gamma) \rightarrow \mathbf{H}_\times^{-\frac{1}{2}}(\mathbf{curl}_\Gamma, \Gamma) \\ \mathbf{\Theta}_2 &: \mathbf{H}_\times^{-\frac{1}{2}}(\mathbf{curl}_\Gamma, \Gamma) \rightarrow \mathbf{H}_\times^{-\frac{1}{2}}(\mathbf{Div}_\Gamma, \Gamma), \end{aligned}$$

such that

$$\mathbf{V}_\varepsilon = \mathbf{\Theta}_2 \mathbf{\Lambda}_{1,\varepsilon}^{-1} \mathbf{\Lambda}_{2,\varepsilon} \mathbf{\Theta}_1 : \mathbf{H}_\times^{-\frac{1}{2}}(\mathbf{Div}_\Gamma, \Gamma) \rightarrow \mathbf{H}_\times^{-\frac{1}{2}}(\mathbf{Div}_\Gamma, \Gamma) \quad (14)$$

can be used as a preconditioner. Such maps can be defined conveniently, depending on the discrete spaces used as it will be shown in next sections.

From the definition of \mathbf{V}_ε (14), the inverse of this operator can also be found: $\mathbf{V}_\varepsilon^{-1} = \mathbf{\Theta}_2 \mathbf{\Lambda}_{2,\varepsilon}^{-1} \mathbf{\Lambda}_{1,\varepsilon} \mathbf{\Theta}_1$.

3.3 Padé approximation of the MtE operator ($\tilde{\mathbf{V}}_\varepsilon^{-1}$)

Regarding the implementation of $\mathbf{V}_\varepsilon^{-1}$, $\mathbf{\Lambda}_{2,\varepsilon}$ is a local symmetrical operator that can be easily approximated. However, $\mathbf{\Lambda}_{1,\varepsilon}$ is a non-local pseudodifferential operator whose calculation is not given straightforward. To overcome this problem, a local approximation of $\mathbf{\Lambda}_{1,\varepsilon}$ can be obtained from a rotating branch cut Padé Approximation:

$$(1+z)^{\frac{1}{2}} \approx R_0 - \sum_{j=1}^{N_p} \frac{A_j}{B_j(1+B_j z)}$$

Hence:

$$\tilde{\mathbf{\Lambda}}_{1,\varepsilon} = \left(\mathbf{I} R_0 - \sum_{j=1}^{N_p} \frac{A_j}{B_j} (\mathbf{I} + B_j \mathcal{J})^{-1} \right)$$

Renaming $\mathbf{I} + B_j \mathcal{J}$ as $\mathbf{\Pi}_j$, the Padé approximation of $\mathbf{V}_\varepsilon^{-1}$ can be applied on $\gamma_N^+ \mathbf{u}$ by solving the following ($\tilde{\mathbf{\Lambda}}_{1,\varepsilon} \mathbf{\Theta}_1 \gamma_N^+ \mathbf{u} = \mathbf{\Lambda}_{2,\varepsilon} \mathbf{\Theta}_2 \gamma_t^+ \mathbf{u}$ on Γ):

$$\left(\mathbf{I} R_0 - \sum_{j=1}^{N_p} \frac{A_j}{B_j} \mathbf{\Pi}_j^{-1} \right) \mathbf{\Theta}_1 (\gamma_N^+ \mathbf{u}) = \left(\mathbf{I} - \mathbf{curl}_\Gamma \frac{1}{\kappa^2} \mathbf{curl}_\Gamma \right) \mathbf{\Theta}_2 \gamma_t^+ \mathbf{u} \quad \text{on } \Gamma \quad (15)$$

Defining $\mathbf{y} := \mathbf{\Theta}_1 (\gamma_N^+ \mathbf{u})$ and $\boldsymbol{\phi}^j := \mathbf{\Pi}_j^{-1} \mathbf{y}$, $\mathbf{c} := -(\mathbf{I} - \mathbf{curl}_\Gamma \frac{1}{\kappa^2} \mathbf{curl}_\Gamma) \mathbf{\Theta}_2 \gamma_t^+ \mathbf{u}$ and having in mind (13), (15) becomes:

$$\begin{cases} \mathbf{y} - \frac{1}{R_0} \sum_{j=1}^{N_p} \frac{A_j}{B_j} \boldsymbol{\phi}^j = -\frac{\mathbf{c}}{R_0} \\ \mathbf{y} - [\mathbf{I} + B_j (\mathbf{Grad}_\Gamma \frac{1}{\kappa^2} \mathbf{Div}_\Gamma - \mathbf{curl}_\Gamma \frac{1}{\kappa^2} \mathbf{curl}_\Gamma)] \boldsymbol{\phi}^j = 0 \end{cases} \quad (16)$$

Now, by introducing $\rho^j \in \mathbf{H}_\times^{-\frac{1}{2}}(\Gamma)$, the original weak formulation for $\mathcal{J}(\mathbf{u})$ reads:

$$\begin{aligned} \int_\Gamma \mathcal{J}(\boldsymbol{\phi}^j) \cdot \mathbf{v} d\Gamma &= \int_\Gamma \frac{1}{\kappa_\varepsilon^2} \mathbf{Grad}_\Gamma \rho^j \cdot \mathbf{v} d\Gamma - \frac{1}{\kappa_\varepsilon^2} \int \mathbf{curl}_\Gamma \boldsymbol{\phi}^j \cdot \mathbf{curl}_\Gamma \mathbf{v} d\Gamma, \\ &\quad \text{with } \rho^j = \mathbf{Div}_\Gamma \boldsymbol{\phi}^j \\ \int_\Gamma \rho^j z d\Gamma &= \int_\Gamma \mathbf{Div}_\Gamma \mathbf{u} z d\Gamma = - \int_\Gamma \boldsymbol{\phi}^j \cdot \mathbf{Grad}_\Gamma z d\Gamma \end{aligned}$$

Which in conjunction with (16), it can be rewritten as a system of equations:

$$\begin{cases} \int_\Gamma \mathbf{y} \cdot \mathbf{v} d\Gamma - \frac{1}{R_0} \sum_{j=1}^{N_p} \frac{A_j}{B_j} \int_\Gamma \boldsymbol{\phi}^j \cdot \mathbf{v} d\Gamma = -\frac{\int_\Gamma \mathbf{c} \cdot \mathbf{v} d\Gamma}{R_0} = \mathbf{rhs} \\ \int_\Gamma \mathbf{y} \cdot \mathbf{w}^j d\Gamma - \int_\Gamma \boldsymbol{\phi}^j \cdot \mathbf{w}^j d\Gamma \\ - B_j \left(\int_\Gamma \mathbf{Grad}_\Gamma \rho^j \cdot \mathbf{w}^j d\Gamma - \frac{1}{\kappa_\varepsilon^2} \int \mathbf{curl}_\Gamma \boldsymbol{\phi}^j \cdot \mathbf{curl}_\Gamma \mathbf{w}^j d\Gamma \right) = 0, \\ \int_\Gamma \kappa_\varepsilon^2 \rho^j z^j d\Gamma + \int_\Gamma \boldsymbol{\phi}^j \cdot \mathbf{Grad}_\Gamma z^j d\Gamma = 0 \end{cases} \quad (17)$$

with $j \in \{1, \dots, N_p\}$.

The calculation of \mathbf{c} , follows from composing the weak form of $\mathbf{\Theta}_2$ with the weak form of $\mathbf{\Lambda}_{2,\varepsilon}$:

$$\mathbf{\Lambda}_{2,\varepsilon} = \int_\Gamma \mathbf{w} \cdot \mathbf{v} d\Gamma - \frac{1}{\kappa_\varepsilon^2} \int \mathbf{curl}_\Gamma \mathbf{w} \cdot \mathbf{curl}_\Gamma \mathbf{v} d\Gamma$$

where $\mathbf{u}, \mathbf{v} \in \mathbf{H}_\times^{-\frac{1}{2}}(\text{curl}_\Gamma, \Gamma)$.

As an example of how similar is $\tilde{\mathbf{V}}_{\varepsilon,h,N_p}^{-1}$ to $\mathbf{V}_{\varepsilon,h}^{-1}$ as N_p , figure 1 shows how the spectrum of $\tilde{\mathbf{V}}_{\varepsilon,h,N_p}^{-1}$ converges to $\mathbf{V}_{\varepsilon,h}^{-1}$ as N_p grows.

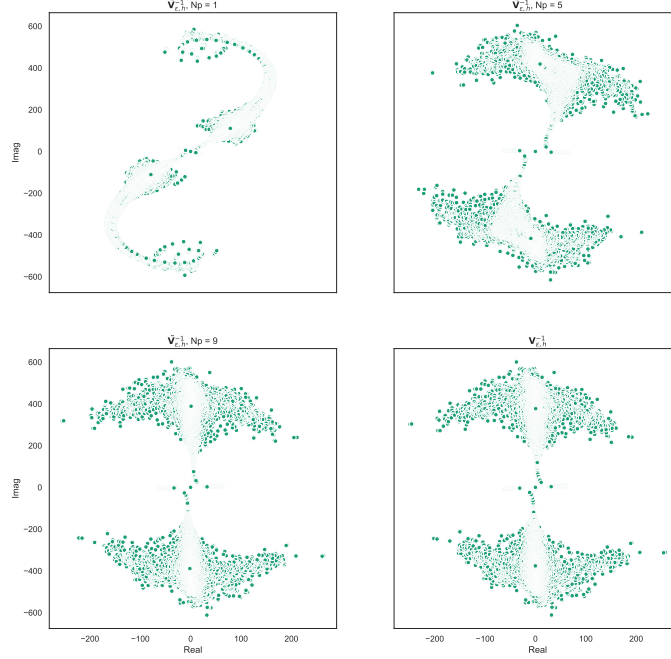


Figure 1: Spectrum comparison for $\mathbf{V}_{\varepsilon,h}^{-1}$ and $\tilde{\mathbf{V}}_{\varepsilon,h,N_p}^{-1}$. Top left: $N_p = 1$. Top right: $N_p = 5$. Bottom left: $N_p = 9$. Bottom right: $\mathbf{V}_{\varepsilon,h}^{-1}$. In all figures, $\kappa = \phi$.

4 Implementation of the discrete MtE preconditioner

To build the discrete approximation of $\tilde{\mathbf{V}}_\varepsilon^{-1}$, consider a polyhedral approximation Γ_h of Γ with a triangulation $\mathcal{T}_h = \cup_{l=1}^{N_T} T^l$. The following discrete spaces are introduced: V_h as the usual Nédélec's space of linear edge finite element defined in [12], R_h as the usual Rao Wilton Glisson's space of linear edge finite element defined in [13] and $Z_h := \{z_h \in \mathbf{H}^{-\frac{1}{2}}(\Gamma_h) | (z_h)|_{T^\ell} \in \mathbb{P}^1(T^\ell), \forall \ell = 1, \dots, N_T\}$ (space of scalar linear basis functions).

Resorting to the same notation used in [9], some discrete operators are needed:

$$\begin{cases} \mathbb{I} = \int_{\Gamma_h} \mathbf{t} \cdot \mathbf{r} d\Gamma_h, & \mathbb{N}_\varepsilon = \int_{\Gamma_h} \frac{1}{\kappa_{\varepsilon,h}^2} \text{curl}_{\Gamma_h} \mathbf{t} \cdot \text{curl}_{\Gamma_h} \mathbf{r} d\Gamma_h \\ \mathbb{K}_\varepsilon = \int_{\Gamma_h} \kappa_{\varepsilon,h}^2 \ell \lambda d\Gamma_h, & \mathbb{L} = \int_{\Gamma_h} \mathbf{Grad}_{\Gamma_h} \ell \mathbf{t} d\Gamma_h \\ \mathbb{I}^M = \int_{\Gamma_h} (\boldsymbol{\nu} \times \mathbf{t}) \cdot \boldsymbol{\gamma} d\Gamma_h \end{cases} \quad (18)$$

where \mathbf{t} and \mathbf{r} belong to V_h , $\boldsymbol{\gamma}$ belongs to R_h and ℓ, λ belong to Z_h .

Since the aim of this research is to use $\tilde{\mathbf{V}}_\varepsilon^{-1}$ as in (12), it is necessary to focus on the relevant part of the procedure, which is calculating $\tilde{\mathbf{V}}_{\varepsilon,h}^{-1} \mathbf{S}_{\kappa,h}$. From (16) and (12), it is possible to deduce:

$$\begin{aligned} (\boldsymbol{\Theta}_{2,h} \boldsymbol{\Lambda}_{2,\varepsilon,h}^{-1}) \left(R_0 \mathbb{I} - \sum_{j=1}^{N_p} \frac{A_j}{B_j} \boldsymbol{\Pi}_{j,\varepsilon,h}^{-1} \right) \boldsymbol{\Theta}_{1,h} (\mathbf{S}_{\kappa,h} (\gamma_N^+ \mathbf{u})_h) \\ = \tilde{\mathbf{V}}_{\varepsilon,h}^{-1} \left(\frac{\mathbb{I}}{2} + \mathbf{C}_{\kappa,h} \right) (\gamma_t^+ \mathbf{u})_h = \mathbf{rhs}_h \end{aligned}$$

From (17) the discrete formulation of Π_j ($\Pi_{j,\varepsilon,h}$) can be written in matricial form as:

$$\begin{bmatrix} (\mathbb{I}^T - B_j \mathbb{N}_\varepsilon) & B_j \mathbb{L} \\ \mathbb{L}^T & \mathbb{K}_\varepsilon \end{bmatrix} \begin{bmatrix} \phi_h^j \\ \rho_h^j \end{bmatrix} = \begin{bmatrix} \mathbf{rhs} \\ 0 \end{bmatrix} \quad (19)$$

Therefore, a block matrix inversion can be performed to get:

$$\Pi_{j,\varepsilon,h} = [\mathbb{I} - B_j(\mathbb{N}_\varepsilon + \mathbb{L}\mathbb{K}_\varepsilon^{-1}(\mathbb{L})^T)] \quad (20)$$

Which gives a first insight for the implementation of $\tilde{\mathbf{V}}_{\varepsilon,h}^{-1}$.

Finally, the discrete preconditioned formulation is given by:

$$(\Theta_{2,h} \Lambda_{2,\varepsilon,h}^{-1}) \left(R_0 \mathbb{I} - \sum_{j=1}^{N_p} \frac{A_j}{B_j} \Pi_{j,\varepsilon,h}^{-1} \right) \Theta_{1,h} \mathbf{S}_{\kappa,h} \underbrace{(\gamma_N^+ \mathbf{u})_h}_{\mathbf{y}} = \mathbf{rhs}_h$$

We must be careful with the operator products in the discretisation. Naively, we would introduce Gram matrices to evaluate the product between $\tilde{\mathbf{V}}_{\varepsilon,h}^{-1}$ and $\mathbf{S}_{\kappa,h}$. However, due to the nature of RWG spaces, some of these are singular, but luckily, it turns that they are not needed in practice. Notice that when defining $\Theta_{1,h}$ one must pay attention to the fact that $\Pi_{j,\varepsilon,h}^{-1}$ maps from the Nédélec space, $\text{SNC} = \nu \times \text{RWG}$, to SNC . Since the test space of $\mathbf{S}_{\kappa,h}$ is also SNC , then $\Theta_{1,h}$ becomes just a standard identity, \mathbf{I} .

$\Theta_{2,h}$ on the other hand is a map from the SNC space to the RWG space. Having in mind that $\text{RWG} = \text{SNC} \times \nu$ then $\Theta_{1,h}$ is just $-\mathbf{I}$.

Finally, we need $\Pi_{j,\varepsilon,h}^{-1}$ to map back to the trial space of space of $\Lambda_{2,\varepsilon,h}^{-1}$ (also the test space of $\mathbf{S}_{\kappa,h}$) so the discrete formulation remains coherent. Thus, we perform the product $\mathbb{I} \Pi_{j,\varepsilon,h}^{-1}$ and the discrete implementation reduces to:

$$-\Lambda_{2,\varepsilon,h}^{-1} \left(R_0 \mathbf{I} - \mathbb{I} \sum_{j=1}^{N_p} \frac{A_j}{B_j} \Pi_{j,\varepsilon,h}^{-1} \right) \mathbf{S}_{\kappa,h} \mathbf{y} = \mathbf{rhs}_h$$

There are 2 ways to solve the discrete problem:

1. Proceed as in [9] and build a block sparse system. Unfortunately, the system generated by this method also had poor spectral properties, so it was discarded as an option.
2. Implement a GMRES iteration using the following algorithm as the matrix-vector product:

Algorithm 1 GMRES matrix-vector product

Input: right hand side \mathbf{y} , discrete operators $\mathbf{S}_{\kappa,h}$, \mathbb{I}^M , and $\mathbf{C}_{\kappa,h}$. LU decomposition of \mathbb{I} , $\Lambda_{2,h}$, and Pade coefficients

$$R_0, \beta_j = -\frac{A_j}{B_j}$$

Output: $r_6 = \tilde{\mathbf{V}}_{\varepsilon,h}^{-1} \mathbf{S}_{\kappa,h} \mathbf{y}$.

- 1: $r_1 = \mathbf{S}_{\kappa,h} \mathbf{y}$.
 - 2: Solve $\Pi_{j,\varepsilon,h} r_2^j = r_1$.
 - 3: $r_3 = \sum_{j=1}^{N_p} r_2^j \beta_j$.
 - 4: $r_4 = R_0 r_1 + \mathbb{I} r_3$.
 - 5: Solve $\Lambda_{2,\varepsilon,h} r_5 = r_4$.
 - 6: $r_6 = -r_5$.
 - 7: **return** r_6
-

(the presence of mass matrices has been omitted here). Notice that in the previous algorithm, all the matrices to be inverted are sparse, except for $\Pi_{j,\varepsilon,h}$, in the third step. Recalling (19):

$$\begin{aligned}
 r_2^j &= \Pi_{j,\varepsilon,h}^{-1} r_1 \equiv \underbrace{\begin{bmatrix} (\mathbb{I} - B_j \mathbb{N}_\varepsilon) & B_j \mathbb{L} \\ \mathbb{L}^T & \mathbb{K}_\varepsilon \end{bmatrix} \begin{bmatrix} r_2^j \\ \rho_h^j \end{bmatrix}}_{(1)} = \begin{bmatrix} r_1 \\ 0 \end{bmatrix} \\
 &\equiv \underbrace{(\mathbb{I} - B_j (\mathbb{N}_\varepsilon + \mathbb{L} \mathbb{K}_\varepsilon^{-1} \mathbb{L}^T))^{-1} r_1}_{(2)}
 \end{aligned}$$

There are different approaches to complete the construction of the GMRES iteration:

- The first method consists of inverting $\Pi_{j,\varepsilon,h}$ using either expression (1) or (2). Notice that solving (1) needs the inversion of a sparse matrix of dimension $(N_e + N_d)^2$ (N_e stands for number of edges and N_d for number of vertices on the grid), but (2) requires the inversion of a dense matrix of dimension N_e , which is as expensive as solving the non regularised EFIE. Hence in 2 a LU decomposition of (1) is passed as an input and a forward-backward substitution is performed in step 3.
- The second method consists of implementing (2), based in the following heuristic, inspired in figure 2 which illustrated the general behavior of Padé coefficients for any N_p .

Notice that when B_j is small, then the value of $\frac{A_j}{B_j}$ becomes big and in this case $\frac{A_j}{B_j} \Pi_{j,\varepsilon,h}^{-1} \approx \frac{A_j}{B_j} \mathbb{I}^{-1}$. On the other hand, when B_j is big, $\frac{A_j}{B_j}$ becomes small and then $\frac{A_j}{B_j} \Pi_{j,\varepsilon,h}^{-1}$ can be neglected.

Hence, we can approximate

$$\sum_{j=1}^{N_p} \frac{A_j}{B_j} \Pi_{j,\varepsilon,h}^{-1} \approx \mathbb{I}^{-1} \sum_{i \in \mathcal{I}} \frac{A_i}{B_i}$$

where \mathcal{I} is a subset of indexes in $\{1, \dots, N_p\}$ such that $|B_j| < \delta$. Therefore, the calculation of (2) reduces to a partial sum of Padé coefficients and the calculation of \mathbb{I}^{-1} .

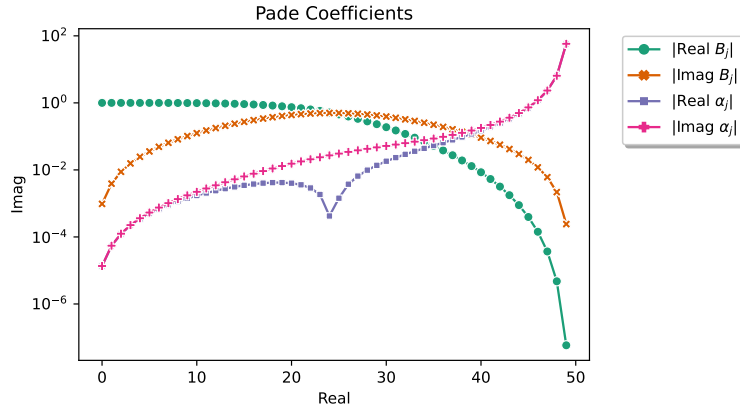


Figure 2: Padé Coefficients $\frac{A_j}{B_j}$ and B_j for $N_p = 50$

Finally, the following summarizes the notation used for each kind of preconditioner:

- $\mathbf{V}_{\varepsilon,h}^{-1}$: MtE approximate operator.
- $\tilde{\mathbf{V}}_{\varepsilon,h,1,N_p}^{-1}$: Padé MtE approximate operator of first type, of order $N_p = n$.
- $\hat{\mathbf{V}}_{\varepsilon,h,2,N_p}^{-1}$: Padé MtE approximate operator of second type, of order $N_p = n$.

5 Numerical Experiments

This section demonstrates the performance of the proposed OSRC preconditioner and some comparisons with other existing preconditioners. All the tests were performed using BEM++ software [14] on a spherical grid of radius $r = 1$.

5.1 $\mathbf{V}_{\varepsilon,h}^{-1}$ Validation

The OSRC operator was validated using the same method as in [9], where bistatic RCS calculated using:

1. A direct formulation of the EFIE (\mathbf{V}_h^{-1}).
2. An approximation of $\mathbf{V}_{\varepsilon,h}^{-1}$ calculated by computing the square roots of the eigenvalues of the matrix that generates $\mathbf{\Lambda}_{1,\varepsilon}$.
3. By applying $\tilde{\mathbf{V}}_{\varepsilon,h,1,2}^{-1}$.

In order to validate the construction of $\tilde{\mathbf{V}}_{\varepsilon,h,1,2}^{-1}$, the calculations of numerical solutions using this operator were compared to analytical solutions on the unit sphere calculated using spherical harmonics.

The first test (figure 3) replicates the results obtained in [9] and shows the bistatic RCS obtained from the scattering problem of an incident electromagnetic plane wave by a PEC unit sphere, for $\kappa = \pi$ and $\kappa = 8\pi$. In both cases, the solution calculated using $\tilde{\mathbf{V}}_{\varepsilon,h,1,2}^{-1}$, is a good approximation of the analytic solution.

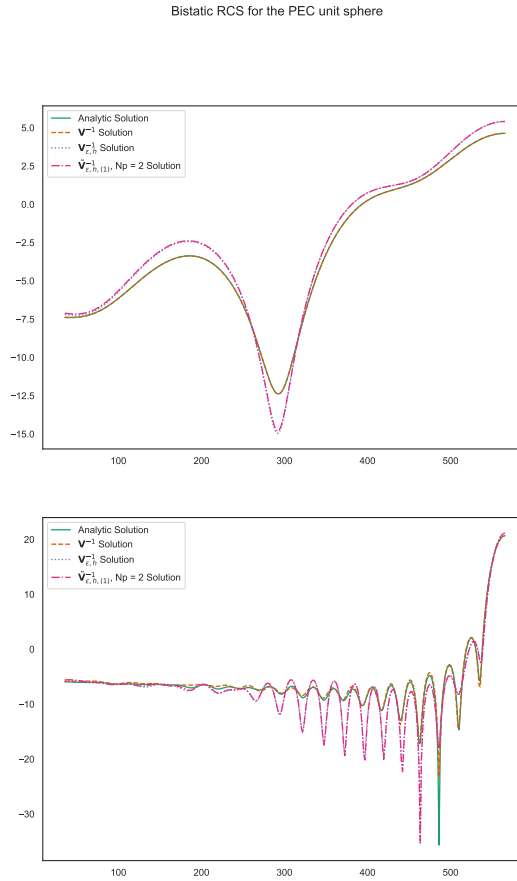


Figure 3: Bistatic RCS for the PEC unit sphere illuminated by an incident electromagnetic plane wave with $\kappa = \pi$ (left) and $\kappa = 8\pi$ (right).

5.2 $\mathbf{V}_{\varepsilon,h}^{-1}$ Performance Comparison

In order to compare the performance of the OSRC preconditioner to existing preconditioners, the following attributes were benchmarked:

- GMRES number of iterations.
- Relative errors between numerical and analytical solutions

- Assembly and solving times for:
 - Pure direct formulation of the EFIE, denoted by $\mathbf{S}_{\kappa,h}$ (always calculated in the primal grid).
 - EFIE preconditioned using the Calderon Multiplicative Preconditioner (CMP), denoted by $\mathbf{S}_{\kappa,h}^2$.
 - EFIE preconditioned with $\tilde{\mathbf{V}}_{\varepsilon,h,1,N_p}^{-1}$, with $N_p = 1, 2$.
 - EFIE preconditioned with $\tilde{\mathbf{V}}_{\varepsilon,h,2,N_p}^{-1}$, with $N_p = 1, 2$. In this case, for $N_p = 1$ we have just one Padé coefficient. When $N_p = 2$ we also only keep just one Padé coefficient because the second coefficient in the expansion is sufficiently small in size to be discarded. We note that this is not identical to the case $N_p = 1$, since the definition of Padé coefficients in [9] shows that these differ when the degree of the expansion (N_p) changes.

These tests were performed using \mathcal{H} -matrix compressions, with $\epsilon = 1E - 5$

Figure 4 shows $\tilde{\mathbf{V}}_{\varepsilon,h,1,*}^{-1} \mathbf{S}_{\kappa,h}$ performs better than $\mathbf{S}_{\kappa,h}^2$ as the number of iterations that takes to solve the system grows at a lower rate. As expected, $\tilde{\mathbf{V}}_{\varepsilon,h,1,*}^{-1} \mathbf{S}_{\kappa,h}$ shows (slightly) better results than $\tilde{\mathbf{V}}_{\varepsilon,h,2,*}^{-1} \mathbf{S}_{\kappa,h}$, because the first is a better approximation than the latter.

Tables 1 shows that $\tilde{\mathbf{V}}_{\varepsilon,h,1,*}^{-1}$ is more efficient in terms of assembly times than the CMP, since $\tilde{\mathbf{V}}_{\varepsilon,h,1,*}^{-1}$ only requires to assemble sparse matrices on the primal grid unlike CMP. Also, table 2 shows that $\tilde{\mathbf{V}}_{\varepsilon,h,1,*}^{-1}$ is more efficient in terms of and solving times, since GMRES iteration is cheaper for sparse matrices.

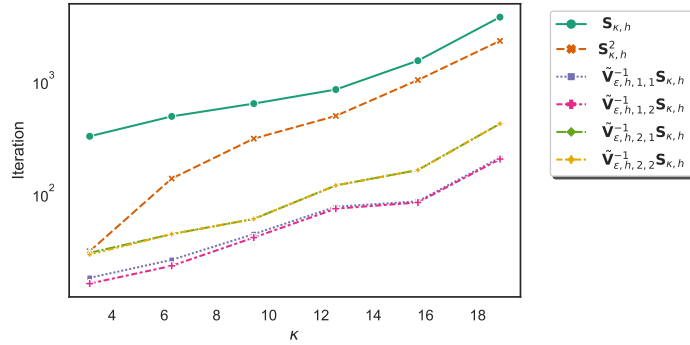


Figure 4: Iterations comparison between different EFIE formulations on a grid with constant relation $\kappa \cdot h$.

Formulation	$\kappa = \pi$	$\kappa = 2\pi$	$\kappa = 3\pi$	$\kappa = 4\pi$	$\kappa = 5\pi$
$\mathbf{S}_{\kappa,h}$	1.000	1.000	1.000	1.000	1.000
$\mathbf{S}_{\kappa,h}^2$	16.095	13.178	19.273	15.738	16.612
$\tilde{\mathbf{V}}_{\varepsilon,h,1,1}^{-1} \mathbf{S}_{\kappa,h}$	1.042	1.098	1.148	1.180	2.571
$\tilde{\mathbf{V}}_{\varepsilon,h,1,2}^{-1} \mathbf{S}_{\kappa,h}$	1.081	1.165	1.265	1.339	1.194
$\tilde{\mathbf{V}}_{\varepsilon,h,2,1}^{-1} \mathbf{S}_{\kappa,h}$	1.007	1.010	1.010	1.012	1.067
$\tilde{\mathbf{V}}_{\varepsilon,h,2,2}^{-1} \mathbf{S}_{\kappa,h}$	1.007	1.009	1.010	1.012	1.025

Table 1: $\mathbf{T}(\mathbf{RS}_{\kappa,h}) / \mathbf{T}(\mathbf{S}_{\kappa,h})$ assembly time ratios comparison between different EFIE formulations on a grid with constant relation $\kappa \cdot h$.

5.3 $\mathbf{V}_{\varepsilon,h}^{-1}$ performance under h refinement.

$\tilde{\mathbf{V}}_{\varepsilon,h,*}^{-1} \mathbf{S}_{\kappa,h}$ should preserve the boundedness of the condition number as $h \rightarrow 0$. It can be seen in figure 5 that the iterations curve of $\tilde{\mathbf{V}}_{\varepsilon,h,2,*}^{-1} \mathbf{S}_{\kappa,h}$ is approximately constant and does not behave worse than the CMP.

In terms of time, table 3 shows that in general, assembling $\tilde{\mathbf{V}}_{\varepsilon,h,*}^{-1} \mathbf{S}_{\kappa,h}$ remains as $h \rightarrow 0$. Table 4 shows that the solving time ratios of $\tilde{\mathbf{V}}_{\varepsilon,h,*}^{-1} \mathbf{S}_{\kappa,h}$ improve for smaller h as the number of iterations that takes to solve the problem remains approximately constant. In both regards, assembly and solving time, $\tilde{\mathbf{V}}_{\varepsilon,h,*}^{-1} \mathbf{S}_{\kappa,h}$ outperforms $\mathbf{S}_{\kappa,h}^2$.

Formulation	$\kappa = \pi$	$\kappa = 2\pi$	$\kappa = 3\pi$	$\kappa = 4\pi$	$\kappa = 5\pi$
$\mathbf{S}_{\kappa,h}$	1.000	1.000	1.000	1.000	1.000
$\mathbf{S}_{\kappa,h}^2$	1.801	3.800	9.946	12.627	23.226
$\tilde{\mathbf{V}}_{\varepsilon,h,1,1}^{-1} \mathbf{S}_{\kappa,h}$	0.090	0.088	0.104	0.164	0.235
$\tilde{\mathbf{V}}_{\varepsilon,h,1,2}^{-1} \mathbf{S}_{\kappa,h}$	0.141	0.113	0.129	0.211	0.148
$\tilde{\mathbf{V}}_{\varepsilon,h,2,1}^{-1} \mathbf{S}_{\kappa,h}$	0.104	0.072	0.084	0.155	0.244
$\tilde{\mathbf{V}}_{\varepsilon,h,2,2}^{-1} \mathbf{S}_{\kappa,h}$	0.065	0.071	0.083	0.155	0.273

Table 2: $\mathbf{T}(\mathbf{RS}_{\kappa,h}) / \mathbf{T}(\mathbf{S}_{\kappa,h})$ solving time ratios comparison between different EFIE formulations on a grid with constant relation $\kappa \cdot h$.

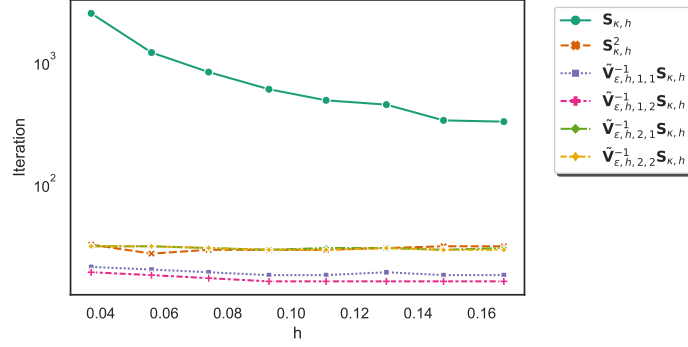


Figure 5: Iterations comparison between different EFIE formulations on a grid with varying discretisation.

Formulation	$h = 0.037$	$h = 0.056$	$h = 0.074$	$h = 0.093$
$\mathbf{S}_{\kappa,h}$	1.000	1.000	1.000	1.000
$\mathbf{S}_{\kappa,h}^2$	22.122	20.792	18.179	14.328
$\tilde{\mathbf{V}}_{\varepsilon,h,1,1}^{-1} \mathbf{S}_{\kappa,h}$	1.128	1.098	1.088	1.072
$\tilde{\mathbf{V}}_{\varepsilon,h,1,2}^{-1} \mathbf{S}_{\kappa,h}$	1.282	1.218	1.198	1.139
$\tilde{\mathbf{V}}_{\varepsilon,h,2,1}^{-1} \mathbf{S}_{\kappa,h}$	1.012	1.010	1.010	1.007
$\tilde{\mathbf{V}}_{\varepsilon,h,2,2}^{-1} \mathbf{S}_{\kappa,h}$	1.012	1.010	1.010	1.008

Table 3: $\mathbf{T}(\mathbf{RS}_{\kappa,h}) / \mathbf{T}(\mathbf{S}_{\kappa,h})$ assembly time ratios comparison between different EFIE formulations on a grid with varying discretisation.

Formulation	$h = 0.037$	$h = 0.056$	$h = 0.074$	$h = 0.093$
$\mathbf{S}_{\kappa,h}$	1.000	1.000	1.000	1.000
$\mathbf{S}_{\kappa,h}^2$	0.409	0.507	0.655	0.713
$\tilde{\mathbf{V}}_{\varepsilon,h,1,1}^{-1} \mathbf{S}_{\kappa,h}$	0.014	0.023	0.039	0.043
$\tilde{\mathbf{V}}_{\varepsilon,h,1,2}^{-1} \mathbf{S}_{\kappa,h}$	0.017	0.029	0.047	0.063
$\tilde{\mathbf{V}}_{\varepsilon,h,2,1}^{-1} \mathbf{S}_{\kappa,h}$	0.014	0.025	0.028	0.051
$\tilde{\mathbf{V}}_{\varepsilon,h,2,2}^{-1} \mathbf{S}_{\kappa,h}$	0.014	0.022	0.028	0.041

Table 4: $\mathbf{T}(\mathbf{RS}_{\kappa,h}) / \mathbf{T}(\mathbf{S}_{\kappa,h})$ solving time ratios between different EFIE formulations on a grid with varying discretisation.

5.4 A final example on a less regular surface.

Finally, the same tests were performed on a NASA almond-shaped grid, to see if the condition number boundedness was preserved on a more interesting shape. Figure 6 shows that even in this case the OSRC preconditioner behaves very similar to the CMP, while being substantially cheaper to compute.

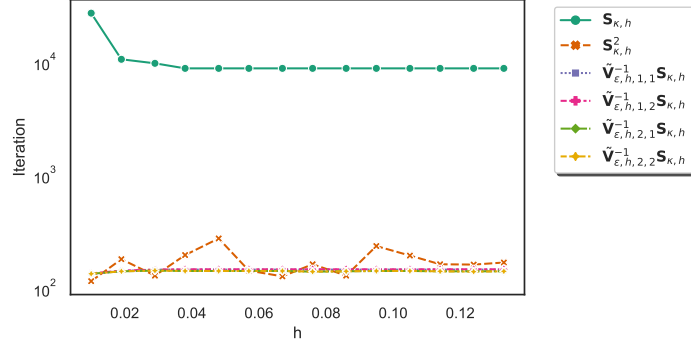


Figure 6: Iterations comparison between different EFIE formulations on an almond-shaped grid with varying h .

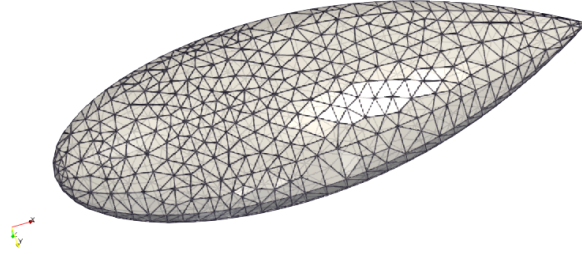


Figure 7: Example of a NASA almond grid.

6 Conclusion

The aim of this paper was to test the an approximation of the Magnetic to Electric operator proposed in [9] as a preconditioner operator for the EFIE. This operator ($\tilde{V}_{\epsilon}^{-1}$) is based on rational complex Padé approximant of an OSRC (V_{ϵ}^{-1}) operator, also proposed in [9].

It was shown that this operator works as a preconditioner for the EFIE and different alternatives for its discretisation were proposed and benchmarked. The results from these tests prove the effectiveness of the proposed preconditioner and that it also outperforms the standard Calderón Multiplicative Preconditioner.

References

- [1] Francesco P Andriulli, Kristof Cools, Hakan Bagci, Femke Olyslager, Annalisa Buffa, Snorre Christiansen, and Eric Michielssen. A multiplicative Calderón preconditioner for the electric field integral equation. *IEEE Transactions on Antennas and Propagation*, 56(8):2398–2412, 2008.
- [2] Xavier Antoine and Marion Darbas. Generalized combined field integral equations for the iterative solution of the three-dimensional helmholtz equation. *ESAIM: Mathematical Modelling and Numerical Analysis*, 41(1):147–167, 2007.
- [3] Xavier Antoine, Marion Darbas, and Ya Yan Lu. An improved surface radiation condition for high-frequency acoustic scattering problems. *Computer Methods in Applied Mechanics and Engineering*, 195(33-36):4060–4074, 2006.
- [4] H. Bagci, F.P. Andriulli, K. Cools, F. Olyslager, and E. Michielssen. A Calderón Multiplicative Preconditioner for the Combined Field Integral Equation. *IEEE Transactions on Antennas and Propagation*, 57(10):3387–3392, oct 2009.
- [5] Timo Betcke, Matthew W. Scroggs, and Wojciech Smigaj. Product algebras for galerkin discretisations of boundary integral operators and their applications. *ACM Trans. Math. Softw.*, 46(1), March 2020.

- [6] Annalisa Buffa and Snorre Christiansen. A dual finite element complex on the barycentric refinement. *Mathematics of Computation*, 76(260):1743–1769, 2007.
- [7] Annalisa Buffa and Ralf Hiptmair. Galerkin boundary element methods for electromagnetic scattering. In *Lecture Notes in Computational Science and Engineering*, pages 83–124. Springer Berlin Heidelberg, 2003.
- [8] M. Darbas, E. Darrigrand, and Y. Lafranche. Combining analytic preconditioner and fast multipole method for the 3-d helmholtz equation. *Journal of Computational Physics*, 236:289–316, 2013.
- [9] Mohamed El Bouajaji, Xavier Antoine, and Christophe Geuzaine. Approximate local magnetic-to-electric surface operators for time-harmonic maxwell’s equations. *Journal of Computational Physics*, 279:241–260, 2014.
- [10] Rainer Kress, V Maz’ya, and V Kozlov. *Linear integral equations*, volume 82. Springer, 1989.
- [11] GREGORYA Kriegsmann, Allen Taflove, and KORADARR Umashankar. A new formulation of electromagnetic wave scattering using an on-surface radiation boundary condition approach. *IEEE Transactions on Antennas and Propagation*, 35(2):153–161, 1987.
- [12] Peter Monk et al. *Finite element methods for Maxwell’s equations*. Oxford University Press, 2003.
- [13] Sadasiva Rao, Donald Wilton, and Allen Glisson. Electromagnetic scattering by surfaces of arbitrary shape. *IEEE Transactions on antennas and propagation*, 30(3):409–418, 1982.
- [14] Matthew W Scroggs, Timo Betcke, Erik Burman, Wojciech Śmigaj, and Elwin van’t Wout. Software frameworks for integral equations in electromagnetic scattering based on calderón identities. *Computers & Mathematics with Applications*, 74(11):2897–2914, 2017.